ELSEVIER

Soil Dynamics and Earthquake Engineering 28 (2008) 387–404

SOIL DYNAMICS AND EARTHQUAKE ENGINEERING

www.elsevier.com/locate/soildyn

Earthquake damage detection in the Imperial County Services Building III: Analysis of wave travel times via impulse response functions

Maria I. Todorovska*, Mihailo D. Trifunac

Department of Civil Engineering, University of Southern California, Los Angeles, CA 90089-2531, USA

Received 4 May 2006; received in revised form 16 June 2007; accepted 1 July 2007

Abstract

The majority of structural health monitoring methods are based on detecting changes in the modal properties, which are *global* characteristics of the structure, and are not sensitive to local damage. Wave travel times between selected sections of a structure, on the other hand, are *local* characteristics, and are potentially more sensitive to local damage. In this paper, a structural health monitoring method based on *changes in wave travel times* is explored using strong motion data from the Imperial Valley Earthquake of 1979 recorded in the former Imperial County Services (ICS) Building, severely damaged by this earthquake. Wave travel times are measured from impulse response functions computed from the recorded horizontal seismic response in three time windows—before, during, and after the largest amplitude response, as determined from previous studies of this building, based on analysis of novelties in the recorded response. The results suggest initial spatial distribution of stiffness consistent with the design characteristics, and reduction of stiffness following the major damage consistent with the spatial distribution of the observed damage. The travel times were also used to estimate the fundamental *fixed-base* frequency of the structure f_1 (assuming the building deformed as a shear beam), and its changes during this earthquake. These estimates are consistent with previous estimates of the soil–structure system frequency, f_{sys}, during the earthquakes ($f_1 < f_{sys}$ as expected from soil–structure interaction studies), and with other estimates of frequency (f_1 from ETABS models, and f_{sys} from ambient vibration tests, and "instantaneous" f_1 from high-frequency pulse propagation).

Keywords: Damage detection; Structural health monitoring; Wave travel times; Deconvolution; Impulse response function; Earthquake response; Wave propagation in structures; Imperial county services building

1. Introduction

Most of the structural health-monitoring methods for civil engineering structures are physically based on detecting changes in the *modal* parameters (frequencies and mode shapes) of the structure, which are *global* properties, depending on the *overall* stiffness of the structure. Hence, they change little when the damage is localized. They are also sensitive to environmental influences (e.g. temperature) and changes in the boundary conditions (e.g. soil–foundation system), which are difficult to separate, and which may produce similar effects as damage on the recorded response (see [1,2] for detailed state of the art reviews on this topic). Despite these known difficulties, the modal methods are still prevailing in structural health monitoring, and most of the recent developments in this field have been in the sensing, data transmission, and computational aspects of the problem. In contrast, this paper deals with the physical aspect of the problem. In particular, it presents an exploratory analysis of a relatively new method for structural health monitoring, based on the wave propagation approach of analysis of the seismic response of structures, which is less common in structural engineering, as opposed to the vibrational approach. Alternatively to mode superposition, the seismic response of a structure can be represented as a superposition of waves that propagate through the structure, reflect from its exterior and interior boundaries and interfere [3–6]. Loss of stiffness due to local damage would cause delays in the wave propagation through the damaged part, which could

*Corresponding author.
E-mail addresses: mtodorov@usc.edu (M.I. Todorovska), trifunac@usc.edu (M.D. Trifunac).

0267-7261/$ - see front matter © 2007 Elsevier Ltd. All rights reserved.
doi:10.1016/j.soildyn.2007.07.001

be detected using seismic response data recorded on each side of the damaged area, along the wave path. A change in wave travel time would depend *only on the changes of the physical properties between the sensors*. Hence, the wave methods should be more sensitive to local damage than the modal methods, and should be able to point out to the location of damage with relatively small number of sensors. Additionally, the local changes in travel time should not be sensitive to the effects of soil–structure interaction, which is a major obstacle for the modal methods based on detecting changes in the structural frequencies.

The spatial resolution of the wave methods would be limited by the number of sensors. Minimum of two sensors (at the base and at the roof) are required to determine if the structure has been damaged, and additional sensors at the intermediate floors would help point out to part of the structure that has been damaged. For example, one additional sensor between these two would help identify if the damage has been in the part of the structure above or beyond that sensor.

This paper explores a relatively new structural health monitoring method, which is a wave method, based on detecting changes in travel times of seismic waves propagating through the structure using impulse response functions. It is based on the premise the loss of stiffness due to damage will lead to decrease of the wave velocity and increase of wave travel time through the damaged part of the structure. The wave travel times are measured by tracing a pulse propagating vertically through the building, which is a virtual pulse generated from the recorded earthquake response by signal processing. In particular these pulses are the impulse response functions of the structure computed by deconvolution of the recorded seismic response at different levels. The wave travel times during the initial time window when the amplitudes of the response are still relatively small are used as baseline. The objective of this paper is to explore if this method would work with actual seismic response data recorded in a building that was damaged during the earthquake, and hence is worth to be further developed and refined. The method is checked by comparison of the delays in arrival times and their spatial distribution, as well as of the inferred reduction of stiffness (assuming uniform mass distribution), with the spatial distribution of the observed damage. The results are also compared with results of other analyses, by translating the changes in wave travel times into changes of the building fundamental fixed-base frequency. The structure to which the method is applied is the former Imperial County Services (ICS) Building—a 6-story reinforced concrete structure in El Centro, California—severely damaged by the Imperial Valley earthquake of October 15, 1979 ($M_L = 6.6$, depth $H = 8$ km), and later demolished. The closest distance from the rupture to the building was only 7 km. The structure was instrumented by a 13 channel accelerograph array, and a free-field site, which all recorded the earthquake. The building transverse (NS) response was recorded along three vertical arrays (at both ends and at the center), which enabled to measure the spatial distribution of the delays in arrival time. A description of the spatial distribution and degree of damage is available for this building. The ICS building is a rare case of an instrumented building severely damaged by an earthquake. No other earthquake records are available in this building.

This paper is the third in a sequel of applications of different structural health monitoring methods to this building used as a benchmark [7,8]. The first paper [7] presents an analysis of the changes in the apparent building frequency with time, and of the inter-story drifts estimated form the strong motion data. It also presents a summary of the description of the building, observed damage following an inspection after the earthquake [9], and the recorded strong motion data. The second paper [8] presents an analysis of novelties (abrupt changes) in the recorded seismic response using expansion in a basis of bi-orthogonal wavelets. This paper compares the results obtained by the different methods in this sequel of papers, and also with other published results, e.g. of response of equivalent linear models using ETABS [9].

The method presented in this paper differs from the wave methods used in non-destructive testing (NDT) of materials in that the latter typically use: (1) ultrasonic waves, which are attenuated quickly along the wave path, (2) need an actuator to create such waves, and (3) detect cracks, or some other defect in a member, using *reflected* waves from the defects. These methods are typically used locally, to detect the location of a defect in a member, but are impractical and too costly for global structural health monitoring [1]. The method in this paper uses seismic waves, which are long (5–500 m) and are not much attenuated, does not need actuators, and is based on measurements of travel times of waves *transmitted* through the damaged zone.

There have been only a few publications in literature on wave propagation methods, other than NDT, for structural health monitoring and damage detection in civil structures [10–15]. Şafak [10] proposed a layered continuous model for analysis of seismic response of a building, and detection of damage by tracing changes in the parameters in the different layers. Ivanović et al. [11] and Trifunac et al. [12] used strong motion data recorded in a 7-story RC building in Van Nuys during the 1994 Northridge earthquake, to explore two methods, one based on travel times estimated using cross-correlation, and the other one based on detecting changes in wave numbers (inversely proportional to the wave velocities) of waves propagating between different levels. Ma and Pines [13] proposed a method based on a lumped mass building model, and propagation of dereverberated waves to identify the damage, which they tested on simulated building response data. Oyunchimeg and Kawakami [14] applied the evolutionary normalized input–output normalization (NIOM) method to earthquake response data recorded in buildings in the Los Angeles area and measured wave travel times through the

buildings, some of which have been damaged and some not damaged by the earthquake. The evolutionary NIOM method gives essentially the impulse response in moving windows in time, and differs from ordinary deconvolution in that it suppresses the high frequencies in the recorded response, and minimizes simultaneously the energy of the input and outputs. If some of the parameters used are set to zero, then the NIOM method gives exactly the impulse response function [16]. Their study shows a substantial increase in the wave travel time during the earthquake shaking for the damaged buildings, and only a small increase for the undamaged ones, and hence shows that changes in wave travel time is related to the changes in structural properties and the state of damage of the building. Hence, the method used in this paper is similar to the one used in Ref. [14], but the case study is different, as well as the level of detail of the analysis. While in Ref. [14] more cases are studied, in this paper one building is studied but in much greater detail. Finally, Todorovska and Trifunac [15] apply the same method of analysis as in this paper to the EW response of the Van Nuys 7-story hotel recorded during 11 earthquakes over a period of 24 years, two of which (1994 Northridge and 1971 San Fernando) damaged the building. They show that substantial increase in wave travel times (decrease in stiffness) was observed only during the earthquakes that caused damage. They also show that the increase in wave travel time and the inferred decrease in the fundamental fixed-base frequency was grater during the first damaging earthquake than during the second one, even though the damage during the latter was more severe, which indicates that the changes in the building due to damage depend on the prior exposure to strong shaking. Finally they show that monitoring changes in the fundamental fixed-base frequency, inferred from wave travel times, is more reliable for structural health monitoring than monitoring changes in the apparent system frequency, which is the one measured from various energy distributions.

Similar wave travel time analyses (using deconvolution or the NIOM method) of buildings that have not been damaged include Kawakami and Oyunchimeg [17,18], Snieder and Şafak [6], and Kohler et al. [19]. These studies show that the wave travel times reflect well the characteristics of the buildings studied.

2. Methodology

2.1. One-dimensional continuous wave propagation model of a building

The nature of wave motion is such that *long enough* waves see a discrete medium they propagate through as a "continuum." In fact, there is no such thing as continuum literally, as at the finest scale, all materials are discrete, i.e. made of atoms, which can further be decomposed into elementary particles. Hence, the seismic waves that are much longer than the dimensions of the discontinuities in a building would see it as a continuum. The simplest continuous model of a narrow building is a shear beam [3], and that of a long building is a shear plate [20]. If the mass and stiffness of the individual stories varies, then horizontally layered models, with piecewise continuous properties can be used, with interfaces at the floor slabs [21–23]. Within a layer that is "homogeneous", the wave paths will be straight lines, and at an interface between two different media, an incident wave will split into a reflected and a refracted wave. At the stress free boundaries, a wave is totally reflected. Deviation from a straight line of propagation (i.e. diffraction) will occur if there are inhomogeneities along the wave path with size comparable to the wavelength of the propagating wave. Finally, such inhomogeneities would appear as infinite barriers to very short waves [22].

In a narrow building, deforming mainly in shear, the deformation due to horizontal earthquake ground motion can be modeled as one-dimensional (1D) wave propagation. The same holds for a long regular building if the disturbance is homogeneous horizontally. The simplest such model is that of an equivalent uniform shear beam. Such a beam is traversed by infinitely many trains of waves, propagating upward and downward, each resulting from a direct incidence, or from a different generation reflection from the stress free boundary at the top, or from the interface with the ground at the bottom. Asymptotic formulae for the infinite sums were presented by Kanai [3] for the undamped case, and by Snieder and Şafak [6] for the damped case, who also prove the equivalence of wave and mode superposition representations. In a layered model, the representation would be more complex, due to reflections and refractions of each wave at each one of the interfaces, with the reflection and transmission coefficients depending on the impedance contrast. This is schematically illustrated in Fig. 1, where the ground is represented as another layer.

An input wave at the base will propagate upward and will be seen *delayed* and attenuated (due to material

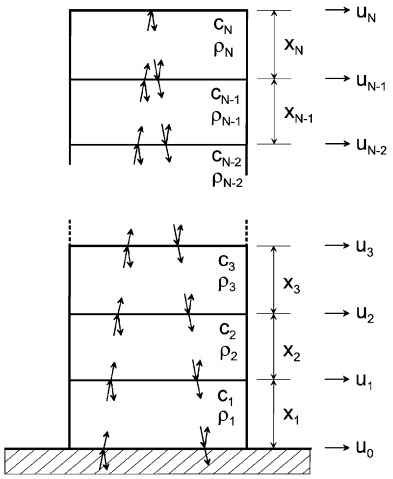

Fig. 1. The model.

damping and reverberations due to reflections from the layer boundaries) at observation points at different heights along the building. At the top, it will be reflected back, and will be seen delayed at consecutive observation points down towards the base. After hitting the base, it will be partially reflected and will again propagate upwards. After many such reflections, the motion resulting from constructive interference will dominate the response. The time delay between the motions at different stories can be observed by a naked eye in some earthquake records in tall buildings, but, to measure such delays, it is more convenient to use some signal processing tool, the most common one being *cross-correlation* analysis. In this paper we use *deconvolution* analysis, as follows.

Let us view the building as a linear time-invariant system, with a single input—the ground motion, $u_{\text{ref}}(t)$, and multiple outputs—the story responses, $u_i(t)$. The input and outputs are related in the time domain by

$$u_i(t) = (u_{\text{ref}} * h_i)(t) = \int_0^t u_{\text{ref}}(\tau) h_i(t-\tau)\,\mathrm{d}\tau \tag{1}$$

and in the frequency domain by

$$\hat{u}(\omega) = \hat{u}_{\text{ref}}(\omega)\hat{h}_i(\omega), \tag{2}$$

where * indicates convolution, and the hat indicates Fourier transform. Function $h_i(t)$ is the impulse response function, and represents the response at level i to input that is a Dirac delta function, $\delta(t)$, that is

$$u_{\text{ref}}(t) = \delta(t) \Leftrightarrow u_i(t) = h_i(t). \tag{3}$$

Function $\hat{h}_i(\omega)$ is the transfer function between the response at level i and the input, and represents the Fourier transform of the response to input such that $\hat{u}_{\text{ref}}(\omega) = 1$. The transfer function is the Fourier transform of the impulse response function

$$\hat{h}_i(\omega) = \mathrm{FT}\{h_i(t)\}. \tag{4}$$

Hence, the impulse response functions can be computed from any recorded response, by taking inverse Fourier transform of the corresponding transfer function, and can be conveniently used to numerically simulate the propagation of a pulse through the building, using actual data. The time delays then can be measured using these impulse response functions. We note here that the response at any level can be used as reference motion, in which case the impulse response function for that level would be a Delta-function.

Practically, $h_i(t)$ is computed using

$$h_i(t) = \mathrm{FT}^{-1}\left\{\frac{\hat{u}_i(\omega)\bar{\hat{u}}_{\text{ref}}(\omega)}{\left|\hat{u}_{\text{ref}}(\omega)\right|^2 + \varepsilon}\right\}, \tag{5}$$

where the bar indicates complex conjugate, ε is a regularization parameter used to avoid numerical instability due to division by very small numbers ("zeros" of the Furies spectrum of the input). This regularization is same as in Ref. [6]. It is noted that there was no need to suppress the higher frequencies in the regularized $\hat{h}_i(\omega)$, which is done by the NIOM method. In this paper, we use $\varepsilon = 0.1\bar{P}$ when u_{ref} is the ground floor record, and $\varepsilon = 0.05\bar{P}$ when u_{ref} is the roof record, where $\bar{P}$ is the average power of u_{ref}.

2.2. Damage detection

To identify damage by detecting changes in travel times, some reference travel times are needed to serve as baseline. For continuously monitored buildings, those could be values obtained from weak motion data recorded "immediately" before the earthquake, which can then be compared with values obtained from similar amplitude motions recorded after the earthquake. Also, using recorded strong motion data one could estimate "instantaneous" travel times from windowed data and track its changes vs. time. In this exploratory analysis, we use strong motion data from an earthquake that damaged the building, and three time windows—before, during, and after the occurrence of the major damage. The limits of these time intervals are chosen based on results of an analysis of novelties in the recorded acceleration response [8]. In each window, the analysis would give the properties of an equivalent linear system representing the building in the corresponding time window.

3. Results and analysis

3.1. The Imperial County Services Building

The former ICS Building was a 6-story reinforced concrete structure in El Centro, California. Here we briefly describe the building, instrumentation layout, and the observed damage following the Imperial Valley earthquake of October 15, 1979 ($M_{\text{L}} = 6.6$, depth $H = 8$ km), for convenience and completeness of this presentation. Further details about the design, recorded data and observed damage can be found in Ref. [9].

Fig. 2 shows a photo of a side view of the building, and Fig. 3 shows the foundation (top) and a typical floor (bottom) layouts. The ground floor was 41.70 m (136 ft and 10 in) by 26.02 m (85 ft and 4 in) in plan, and the height of the building was 25.48 m (83 ft and 7 in). The foundation consisted of pile caps resting on Raymond tapered piles which were interconnected by grade beams (Fig. 3, top). Lateral resistance of all levels in the longitudinal (EW) direction was provided by two exterior moment frames at column lines 1 and 4, and two interior moment frames on column lines 2 and 3 (Fig. 3). The lateral resistance in the transverse (NS) direction was not continuous. At the ground floor level, it was provided by four short shear walls located along column lines A, C, D, and E and extending between column lines 2 and 3 only (Fig. 3, top). At the 2nd floor and above, lateral (NS) resistance was provided by two shear walls at the east and west ends of the building (Fig. 3, bottom). This caused the building to appear top heavy with a soft first story (Fig. 2).

Fig. 2. A view (towards North) of the ICS Building.

The irregularities in the NS stiffness at the ground floor appear to have resulted in excessive torsional response and in significant coupling of the NS and torsional excitations and responses. The design strength of the concrete was 34.5 MPa (5 ksi) for columns, 20.7 MPa (3 ksi) for the elements below ground level, and 27.6 MPa (4 ksi) everywhere else. All reinforcing steel was specified to be grade 40 ($F_y = 276$ MPa).

The building was instrumented by a 13 channel accelerograph array, and a free-field site, which all recorded the earthquake. Fig. 4 shows a sketch of the building with the location of the sensors. The film records were digitized and released as 22.5 s of acceleration data equally sampled at 0.02 s, band-pass filtered with Ormsby filters between 0.1–0.125 and 25–27 Hz. The recorded peak accelerations at the roof and ground floor were 571 and

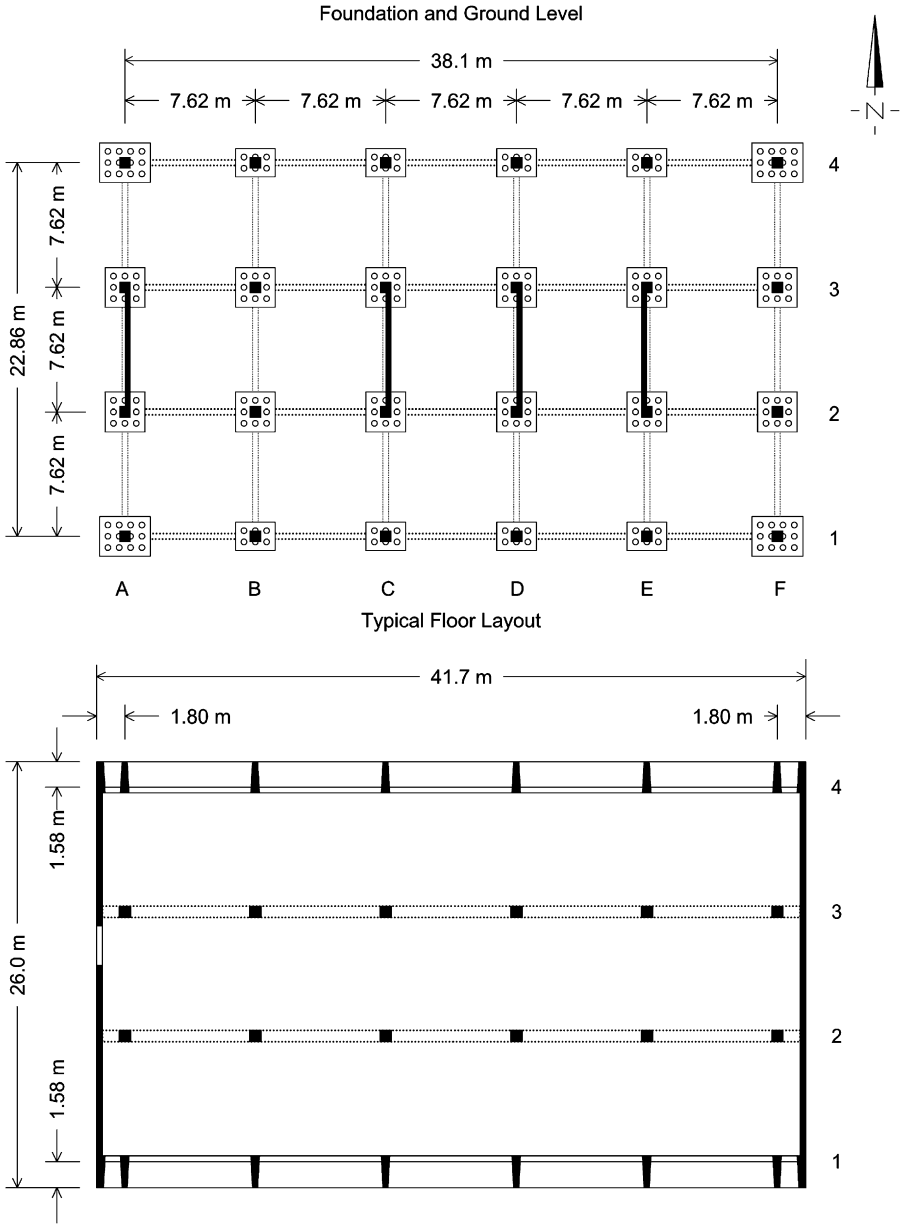

Fig. 3. Foundation and ground level plan (top) and typical floor layout (bottom) of the ICS Building.

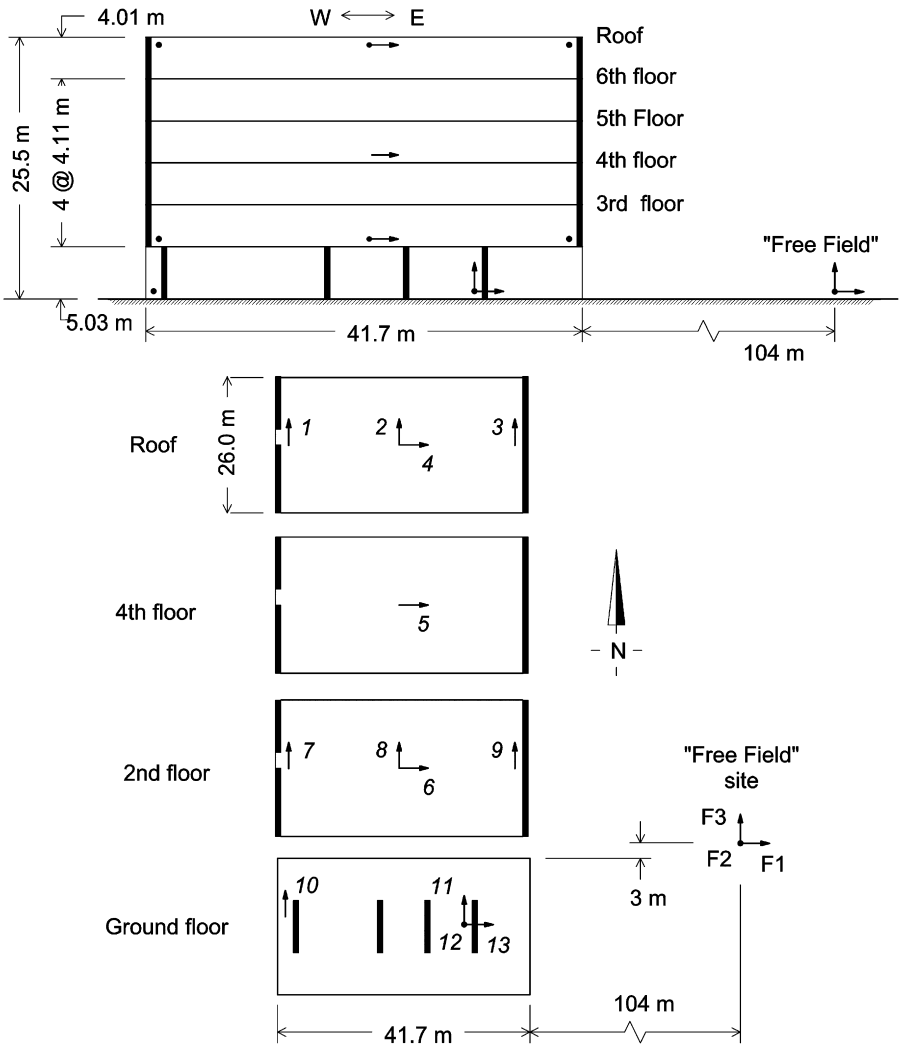

Fig. 4. Layout of the seismic monitoring array in the ICS Building.

339 cm/s^2 in the NS direction and 461 and 331 cm/s^2 in the EW direction. For this analysis, we further high-pass filtered the data at 0.2–0.3 Hz using also an Ormsby filter, and upsampled (by linear interpolation) to 0.01 s. Fig. 5 shows plots of the instrument corrected and band-pass filtered accelerations.

The building was severely damaged by this earthquake, and was later demolished [9]. Fig. 6 shows a schematic representation of the observed damage. The major failure occurred in the columns of frame F (at the east end of the building) at the ground floor. The vertical reinforcement was exposed and buckled, and the core concrete could not be contained, resulting in sudden failure and shortening of the columns subjected to excessive axial loads. This in turn caused an incipient vertical fall of the eastern end of the building, causing cracking of the floor beams and slabs near column line E on the second, third and higher floors. Fig. 7a shows a photo of the damage of columns F1 and F2 at the ground floor, and Fig. 7b shows a closer view of the buckled steel bars of column F1. Columns in lines A, B, D, and E also suffered damage. Columns in frames A and E did not suffer as extensive damage as shortening and buckling of the reinforcement in line F at the east side, but large concrete cracks and exposed reinforcement could be seen near the base. In the columns in interior frames B to E, visible cracks and spalling of the concrete cover were also observed [9].

3.2. Impulse responses and travel times for EW motions

The analysis of novelties in the response of this building [8] suggested that damage first occurred at about 6.4 s, proceeded between 8.2 and 9.2 s, and culminated at about 11.2 s, with the collapse of the first story columns (at line F) at the east side of the building (Figs. 3, 6, and 7a, b). Based on these results, in this paper, we consider three time windows—before, during, and after the major damage occurred: $t<7$ s, $7<t<13$ s, and $t>13$ s. We measure the travel times of the identified pulses for each time window, and analyze the changes relative to the first time window, which we chose to serve as baseline data.

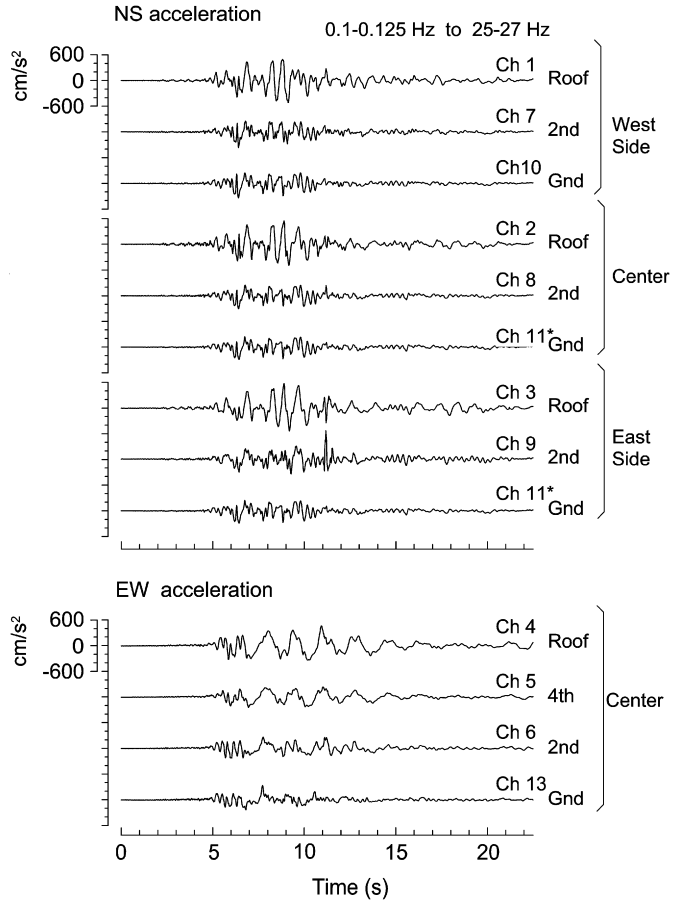

Fig. 5. Accelerations (NS and EW components) recorded in the ICS Building during the 1979 Imperial Valley earthquake.

We first show results for the EW (longitudinal) response of the ICS building, for which a 1D shear wave propagation model is perhaps most appropriate, as the distribution of stiffness in the NS direction was nonsymmetrical, and the contribution of torsion to the recorded NS response was significant [7]. EW motions were recorded at the ground floor (Channel 13), 2nd floor (Channel 6), 4th floor (Channel 5), and the roof (Channel 4) (Fig. 4). Fig. 8 shows impulse response functions for EW motions at different levels in the building, for an input impulse applied at the base (left), and at the roof (right). The different types of lines show results for different time windows. The impulse response functions are shown only for the early stages of response to emphasize the differences in arrival times of the pulses (for the different time windows and at different levels in the building).

The plots on the left-hand side in Fig. 8 show an impulse at time $t = 0$ in the ground floor motion, which propagates up, reaching the upper floors with some time delay, reflects from the roof, and propagates down. The "input" pulse has finite width due to the finite bandwidth of the records, and the regularization parameter ε. The downward propagating pulse is not seen at the ground floor due to the nature of Eq. (5), which always gives an impulse at time $t = 0$, at the level used as reference. Within the time limits of the plots, its reflection from the ground floor can be seen only in the 2nd floor impulse response computed from the data from the first time window ($t < 7$ s).

The plots on the right-hand side in Fig. 8 show an input pulse at time $t = 0$ at roof level, which propagates down with increasing time. Another acausal wave can be seen

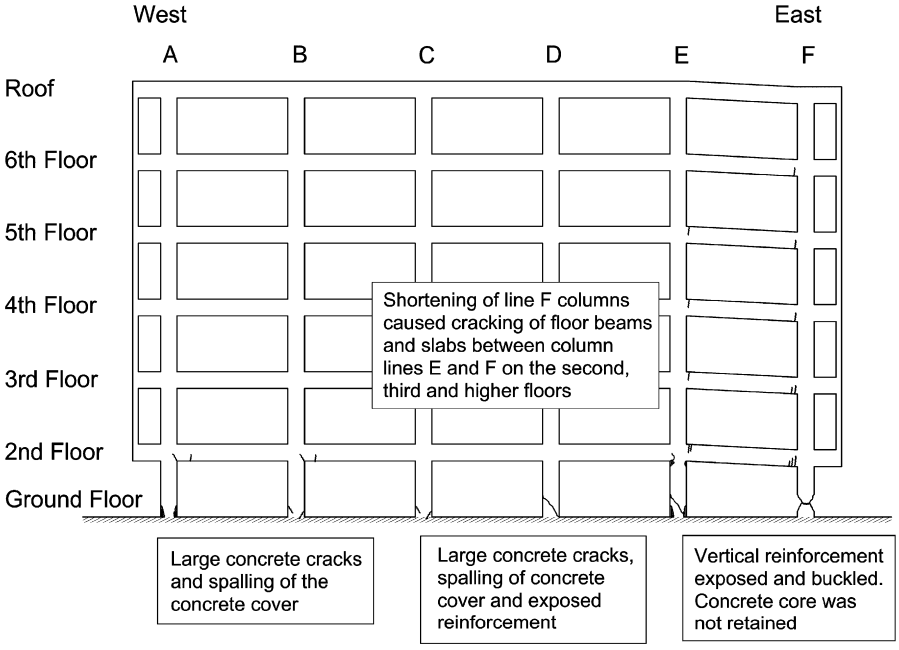

Fig. 6. Schematic representation of the damage in the ICS Building following the 1979 Imperial Valley earthquake (reproduced from Ref. [8]).

Fig. 7. Photographs of damage: columns F1 and F2 at the ground floor (a) and column F1 (b).

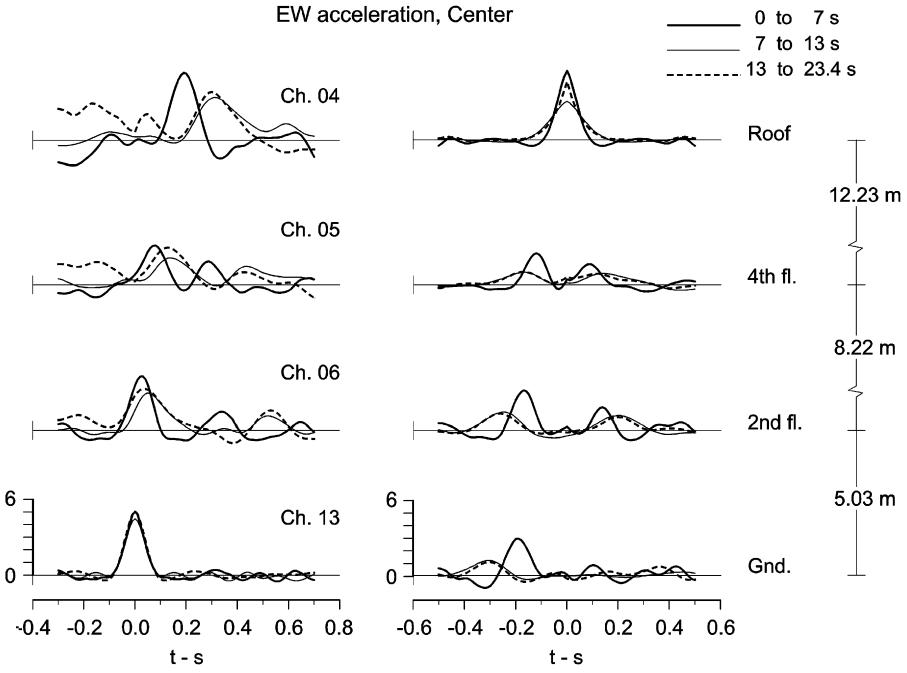

Fig. 8. Impulse response functions for EW motions and for input impulse at the ground floor (left) and at the roof (right).

propagating down in negative time, which corresponds to the upward propagating waves in the physical model. This acausal wave confirms that no matter at which level the "input" pulse is introduced by the data processing, the results reveal the nature of the physical process, which consists of input from the base and total reflection from the roof.

The plots in Fig. 8 show that the travel times of the pulses for the three time windows are different, indicating longer travel times (i.e. reduced stiffness) within the second and third time window ($t>7$ s) as compared to the first time window ($t<7$ s). For this exploratory analysis of the capability of this method to detect damage in real data, we measured the arrival times from the plots of the impulse response functions by visual inspection. The values read are therefore approximate (we estimate the accuracy of reading the arrival times to be about 0.01 s). The travel times can be estimated more accurately by fitting a model to the data, but this is beyond the scope of this paper. The results are tabulated in Table 1. The upper part of this table shows the measurements for an input impulse at the base propagating up (Fig. 8, left), while the lower part—for an input impulse at the roof propagating acausally down (in negative time) (Fig. 8, right). The first column shows: (1) the floor level where the acceleration sensor was located. The following group of two columns shows for $t<7$ s: (2a) the arrival time, t_i, of the pulse at the particular sensor and (2b) the travel time τ_i of the pulse within segment i of the building, consisting of the stories between two sensors. The following two groups of columns (3a,b and 4a,b) show the same quantities, respectively for $7<t<13$ s, and for $t>13$ s. It can be seen from this table that the travel times obtained from the two signal processing experiments are mutually consistent, differing by about 10^{-2} s (which is 5.5% of the travel time through

Table 1
EW motions: measurements of arrival times, t_i, and of wave travel times, τ_i (from the plots in Fig. 7)

		EW motions					
		$t<7$ s		$7<t<13$ s		$t>13$ s	
	(1)	(2a)	(2b)	(3a)	(3b)	(4a)	(4b)
	Floor	t_i (s)	τ_i (s)	t_i (s)	τ_i (s)	t_i (s)	τ_i (s)
Input impulse at Ground floor, pulse going up	Roof	0.17		0.31		0.30	
			0.10		0.17		0.17
	4th	0.07		0.14		0.13	
			0.04		0.09		0.09
	2nd	0.03		0.05		0.04	
			0.03		0.05		0.04
	Ground	0.00		0.00		0.00	
Input impulse at the Roof, acausal pulse going down	Roof	0.00		0.00		0.00	
			0.12		0.18		0.18
	4th	−0.12		−0.18		−0.18	
			0.05		0.07		0.08
	2nd	−0.17		−0.25		−0.26	
			0.02		0.06		0.05
	Ground	−0.19		−0.31		−0.31	

the entire height of the building above ground level). It can also be seen that the travel times increased during the second and third time window, relative to the first one, which indicates softening of the structure, consistent with the occurrence of damage.

3.3. Impulse responses and travel times for NS motions

The NS (transverse) motions were recorded at the ground floor, 2nd floor and roof, along the west side, center and east side of the building. An exception is the ground floor where there were only two sensors, one at the west side, and the other one between the center and east side of the building (Fig. 4). We computed impulse response functions for the NS motions and measured travel times between sensors along each one of the three vertical arrays, and within each one of the three time windows. The results are presented in a similar fashion as for the EW motions (Fig. 8). Figs. 9–11 show impulse response functions respectively for NS motions recorded along the west side (channels 10, 7, and 1, see Fig. 4), the center (channels 11, 8, and 2), and the east side (channels 11, 9, and 3) of the building. The pulse arrival times and travel times between sensors are tabulated in Table 2, which show the same quantities as Table 1. As for the EW motions, the travel times measured from the two signal processing experiments are not only mutually consistent, but are practically identical up to the accuracy of readings (10^{-2} s).

3.4. Mean travel times and inferences on wave velocities and changes in floor stiffness

The mean travel times, τ_i (over the two measurements, see Tables 1 and 2), were calculated and used in the subsequent analysis. The results are tabulated in Table 3 for EW motions and in Table 4 for NS motions. The first two columns in these tables show: (1) the floor level and (2) the distance between neighboring sensors, h_i. The following group of three columns shows for $t<7$ s: (3a) the mean travel time τ_i, (3b) $4\tau_i$ (= contributions from section i to the fundamental period of vibration of an equivalent uniform shear beam model of the building), and (3c) the average (over the floors within segment i) velocity of wave propagation, $v_i = h_i/\tau_i$. The values of v_i for this particular time interval were used as *baseline* in analyzing the changes. The next two groups of five columns correspond respectively to time windows $7<t<13$ s, and $t>13$ s. The first three columns in each group show the same quantities as columns (3a), (3b) and (3c). The additional two columns show the changes in: ((4d) and (5d)) the wave velocities and ((4e) and (5e)) the rigidities relative to the baseline (the corresponding values for the first time interval, $t<7$ s). The change in velocities can be directly computed from the travel times as $\Delta v_i/v_{\text{ref}} = (v_i - v_{\text{ref}})/v_{\text{ref}} = \tau_{\text{ref}}/\tau_i - 1$. The change of rigidity was estimated based on the fact that, for almost uniform distribution of density along the height of the building, $\mu_i \sim v_i^2$, where μ_i is the shear modulus for segment i of the building. Then $\Delta\mu_i/\mu_{\text{ref}} = (\tau_{\text{ref}}/\tau_i)^2 - 1$.

The results in Tables 3 and 4 are shown graphically in Figs. 12–14, and are discussed in Sections 3.4.1 and 3.4.2. First, the consistency of the initial estimates of the floor shear wave velocities is examined. Then the changes in floor stiffness vs. time, and their spatial distribution are discussed.

3.4.1. Initial shear wave velocities

Fig. 12 shows schematically the spatial distribution of the "initial" (i.e. representative values for time window

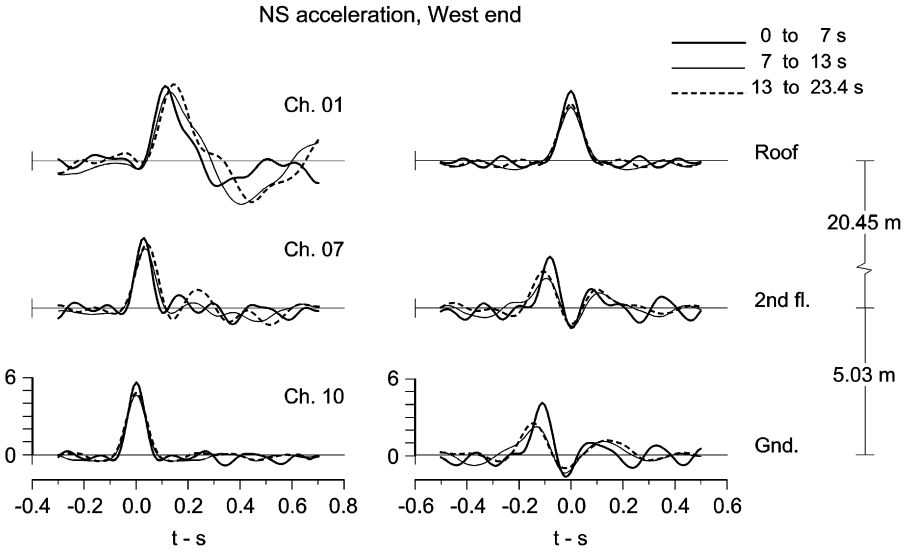

Fig. 9. Same as Fig. 8 but for NS motions recorded at the west side of the building.

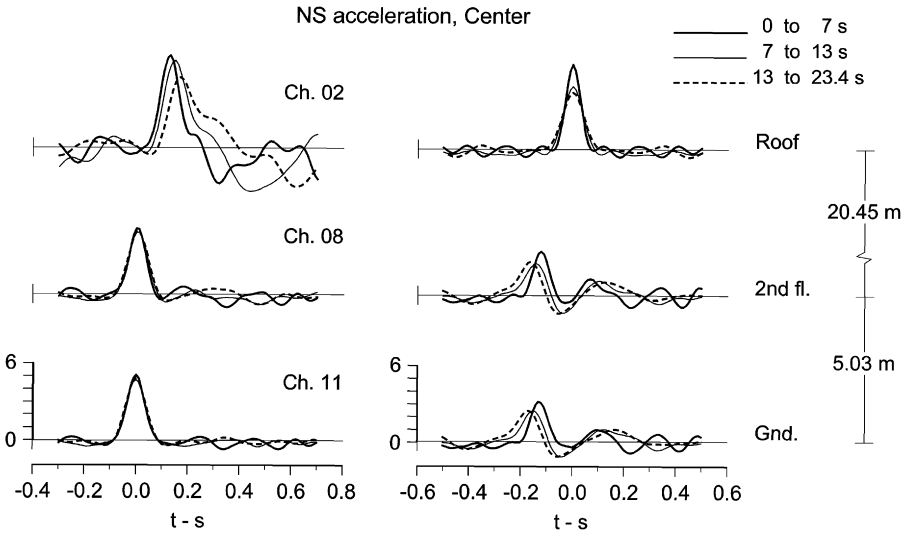

Fig. 10. Same as Fig. 8 but for NS motions recorded at the center of the building.

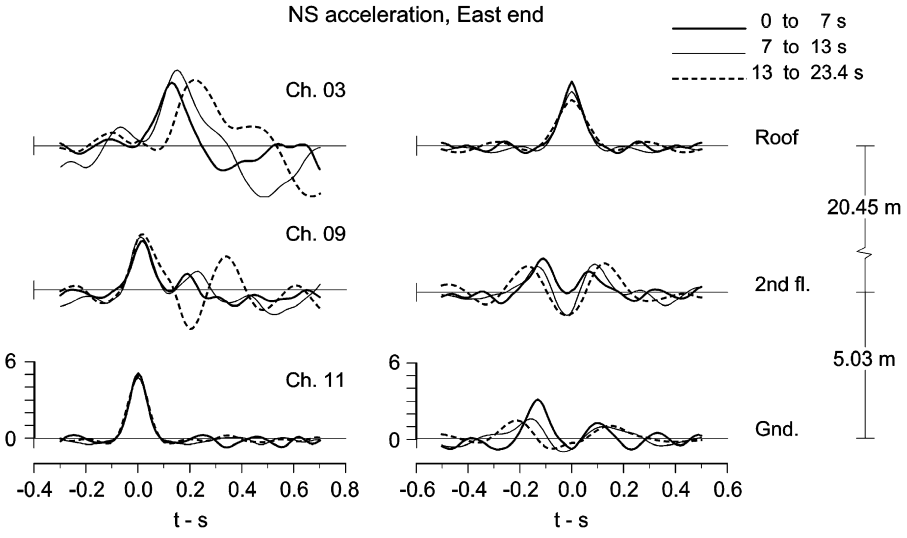

Fig. 11. Same as Fig. 8 but for NS motions recorded at the east side of the building.

Table 2
NS motions recorded at the west side, center, and east side of the building: measurements of arrival times, t_i, and of wave travel times, τ_i (from the plots in Figs. 8–10)

		NS motions					
		$t<7$ s		$7<t<13$ s		$t>13$ s	
	(1)	(2a)	(2b)	(3a)	(3b)	(4a)	(4b)
	Floor	t_i (s)	τ_i (s)	t_i (s)	τ_i (s)	t_i (s)	τ_i (s)
West end							
Input impulse at Ground floor, pulse going up	Roof	0.11		0.13		0.15	
			0.08		0.095		0.11
	2nd	0.03		0.035		0.04	
			0.03		0.035		0.04
	Ground	0.00		0.00		0.00	
Input impulse at the Roof, acausal pulse going down	Roof	0.00		0.00		0.00	
			0.08		0.10		0.11
	2nd	−0.08		−0.10		−0.11	
			0.03		0.03		0.04
	Ground	−0.11		−0.13		−0.13	
Center							
Input impulse at Ground floor, pulse going up	Roof	0.13		0.15		0.17	
			0.12		0.14		0.16
	2nd	0.01		0.01		0.01	
			0.01		0.01		0.01
	Ground	0.00		0.00		0.00	
Input impulse at the Roof, acausal pulse going down	Roof	0.00		0.00		0.00	
			0.12		0.14		0.16
	2nd	−0.12		−0.14		−0.16	
			0.01		0.01		0.01
	Ground	−0.13		−0.15		−0.17	
East end							
Input impulse at Ground floor, pulse going up	Roof	0.13		0.15		0.22	
			0.11		0.13		0.19
	2nd	0.02		0.02		0.03	
			0.02		0.02		0.03
	Ground	0.00		0.00		0.00	
Input impulse at the Roof, acausal pulse going down	Roof	0.00		0.00		0.00	
			0.11		0.14		0.17
	2nd	−0.11		−0.14		−0.17	
			0.02		0.02		0.05
	Ground	−0.13		−0.16		−0.22	

$t<7$ s) shear wave velocities, v_i, that are tabulated in Table 3. These represent the average floor velocities between two sensors.

The results for EW motions (Table 3; Fig. 12, left) indicate initial wave velocities of 201 m/s through the 1st floor, 183 m/s between the 2nd and 4th floors, and 111 m/s between the 4th floor and roof. The velocity of an equivalent uniform shear bream is 142 m/s.

The results for NS motions at the west side of the building (Table 4, top; Fig. 12, right) imply initial velocities of 168 m/s through the 1st floor, and 256 m/s through the upper part. The higher velocity in the upper part is due to the end shear wall, which extended throughout the entire width of the building, while the one at the 1st floor extended only along one third of the width (see Fig. 3). The velocity of an equivalent uniform shear beam is 232 m/s.

The results for NS motions at the center of the building (Table 4, center; Fig. 12, right) imply initial velocity of 503 m/s through the 1st floor, and 170 m/s in the upper part. The velocity of an equivalent uniform shear beam is 196 m/s. The larger value for the 1st floor than for the upper floors can be explained by the added stiffness from the three shear walls near the sensors, which extended only over the height of the 1st floor, while there was no shear wall in the upper part of the building between the sensors.

The results for NS motions at the east end of the building (Table 4, bottom; Fig. 12, right) imply initial velocity of 252 m/s through the 1st floor, and 186 m/s in the upper part. This is opposite of what one would expect, that

Table 3
EW motions: mean travel times τ_i (over the two measurements; see top and bottom parts of Table 1), average wave velocities for the segments of the building between sensors, v_i, and percent changes in these velocities and corresponding rigidities (relative to time interval $t<7$ s)

		EW motions												
		$t<7$ s			$7<t<13$ s					$t>13$ s				
(1)	(2)	(3a)	(3b)	(3c)	(4a)	(4b)	(4c)	(4d)	(4e)	(5a)	(5b)	(5c)	(5d)	(5e)
Floor	h_i (m)	τ_i (s) (mean)	$4\tau_i$ (s)	v_i (m/s) $= v_{ref}$	τ_i (s) (mean)	$4\tau_i$ (s)	v_i (m/s)	$\Delta v_i/v_{ref}$ (%)	$\Delta\mu_i/\mu_{ref}$ (%)	τ_i (s) (mean)	$4\tau_i$ (s)	v_i (m/s)	$\Delta v_i/v_{ref}$ (%)	$\Delta\mu_i/\mu_{ref}$ (%)
Roof	12.23	0.110	0.44	111	0.175	0.70	70	−37	−60	0.175	0.70	70	−37	−60
4th	8.22	0.045	0.18	183	0.080	0.32	103	−44	−68	0.085	0.34	97	−47	−72
2nd	5.03	0.025	0.10	201	0.055	0.22	91	−55	−80	0.045	0.18	112	−44	−69
Ground														

Table 4
NS motions recorded at the west side, center and east side of the building: mean travel times τ_i (over the two measurements, see Table 2), average wave velocities for the segments of the building between sensors, v_i, and percent changes in these velocities and corresponding rigidities (relative to time interval $t<7$ s)

		NS motions at West end												
		$t<7$ s			$7<t<13$ s					$t>13$ s				
(1)	(2)	(3a)	(3b)	(3c)	(4a)	(4b)	(4c)	(4d)	(4e)	(5a)	(5b)	(5c)	(5d)	(5e)
Floor	h_i (m)	τ_i (s) (mean)	$4\tau_i$ (s)	v_i (m/s) $= v_{ref}$	τ_i (s) (mean)	$4\tau_i$ (s)	v_i (m/s)	$\Delta v_i/v_{ref}$ (%)	$\Delta\mu_i/\mu_{ref}$ (%)	τ_i (s) (mean)	$4\tau_i$ (s)	v_i (m/s)	$\Delta v_i/v_{ref}$ (%)	$\Delta\mu_i/\mu_{ref}$ (%)
West end														
Roof	20.45	0.08	0.32	256	0.098	0.39	209	−18	−33	0.11	0.44	186	−27	−47
2nd	5.03	0.03	0.12	168	0.032	0.13	157	−7	−13	0.04	0.16	126	−25	−44
Ground														
Center														
Roof	20.45	0.12	0.48	170	0.14	0.56	146	−14	−26	0.16	0.64	128	−25	−43
2nd	5.03	0.01	0.04	503	0.01	0.04	503	0	0	0.01	0.04	503	0	0
Ground														
East end														
Roof	20.45	0.11	0.44	186	0.135	0.54	151	−19	−34	0.18	0.72	114	−39	−63
2nd	5.03	0.02	0.08	252	0.02	0.08	252	0	0	0.04	0.16	126	−50	−75
Ground														

is lower velocity through the 1st floor compared to the upper floors, considering the actual distribution of stiffness (Fig. 3). However, we note that the sensor at the ground floor was not at the east end, but about halfway towards the center, near the last 1st floor shear wall. Hence, the "1st floor velocity" obtained from the travel times is not representative of waves propagating up through the east side, but probably represents waves reaching the 2nd floor through the shear wall near sensor 8 and then propagating horizontally through the "rigid" floor slab. The lower than expected velocity for the upper part of the building is discussed the next paragraph.

Next we compare the initial NS velocities horizontally, examining their variations along the building length. For the upper part, the design drawings show that the actual "stiffness at the center" was smaller than at the ends, and that the stiffness at both ends was very similar. Hence, one would expect smaller velocity at the center and approximately equal velocities at the ends. We also know from the analysis of drifts that they were the smallest at the center and the largest at the east end (see Fig. 7 in Ref. [7]), even

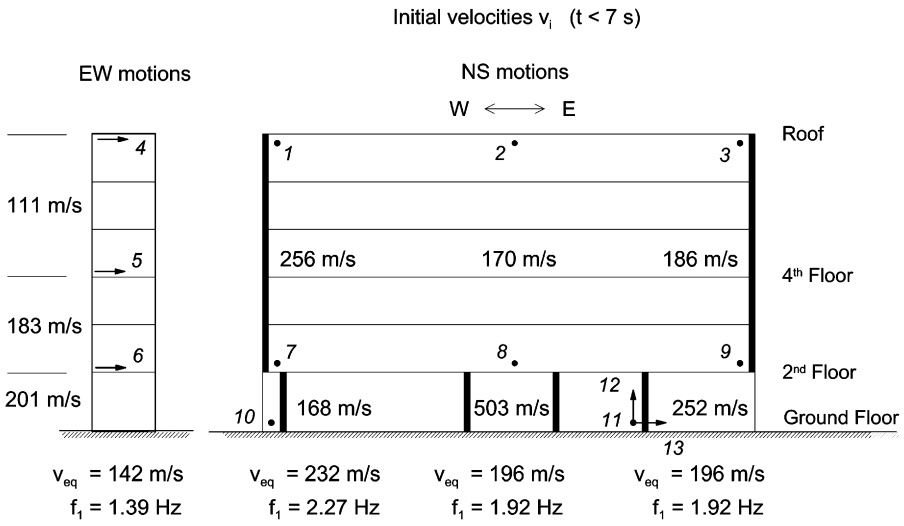

Fig. 12. Initial ($t<7$ s) shear wave velocities, v_i, for different segments of the building. At the bottom, the equivalent shear wave velocities for a uniform shear beam, v_{eq} are given, and the estimated fundamental fixed-base frequencies, f_1.

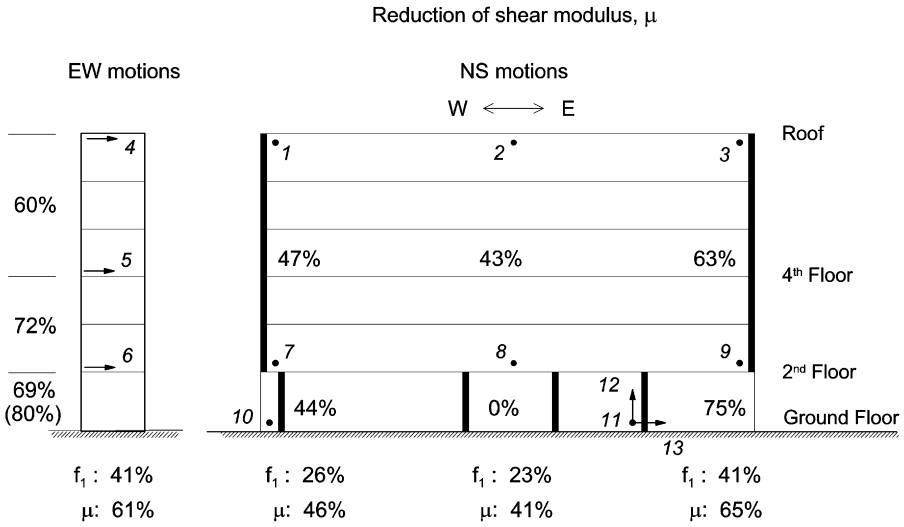

Fig. 13. Final reductions of shear moduli, μ_i, for different segments of the building estimated from changes in travel times. At the bottom, the changes in f_1 and the equivalent shear modulus are shown.

within the initial time window ($t<7$ s), before the severe damage occurred, as a result of the asymmetric distribution of stiffness at the 1st floor. The wave travel times give the smallest velocity at the center, as expected, but somewhat smaller velocity at the east side (186 m/s) than at the west side (256 m/s), which is consistent with the larger drifts at the east end, resulting in a "softer" structure even before the severe damage occurred. If true, the latter suggests strong dependence of the travel times (and inferred velocities), on the level of strain in the structural members.

In the lower part of the building, the design drawings suggest the smallest stiffness at the east end and the largest stiffness at the center, and the analysis of drifts shows largest drifts at the east end and smallest drifts at the center. The travel times give (by far) the largest velocity at the center (503 m/s as compared to 168 m/s at the west end), which is consistent with both the designed stiffness and the observed drifts. The travel times give velocity at the east end (252 m/s) larger than that at the west end, contrary to the expectations, but, as mentioned earlier, the value for the east end may not be representative of waves propagating through the columns of at the east side.

3.4.2. Changes in stiffness

A most important check of the method is that it depicts correctly the *changes* in stiffness in the different parts of the structure. Fig. 13 shows the spatial distribution of the changes is stiffness, $\Delta\mu_i/\mu_{i,\mathrm{ref}}$, computed from the measured changes in travel times, and listed in Tables 3 and 4. The percentages shown represent the changes between the *average* stiffness in the third time window ($t>12$ s) relative to the *average* stiffness in the first time window ($t<7$ s).

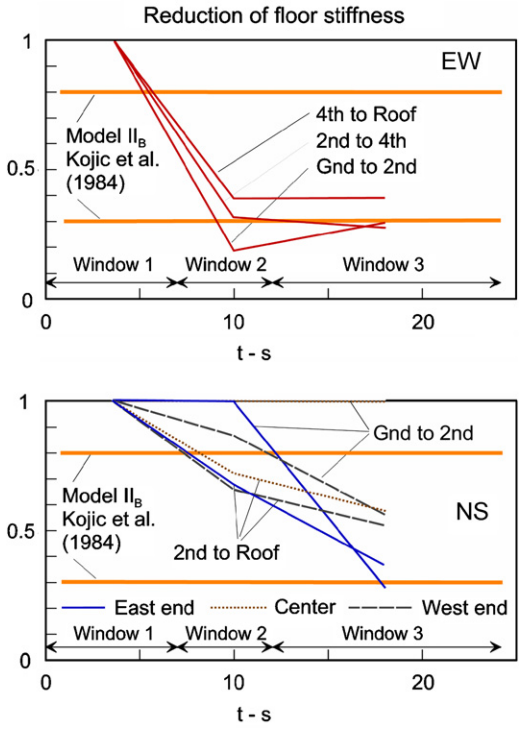

Fig. 14. Reduction of floor stiffness vs. time.

The changes for the EW motions suggest hardening in the 1st floor (by about 10%) during the third time window, following the large (69%) reduction during the second time window. Hence, for this segment of the building, the second interval reduction (80%) is shown in brackets, as the maximum value. At the bottom of Fig. 13, the changes in the fundamental fixed-base frequencies, computed from the total travel times are shown and the implied change of the overall stiffness.

Fig. 13 suggests reduction of stiffness throughout the building between 40% and 80%. For EW motions, the reduction was the largest in the first story (80% during the second time window), but was also large in the upper stories (72% between the 2nd and 4th floors, and 60% between the 4th floor and roof). This is consistent with the spatial distribution of the observed damage (Fig. 6), which was the largest in the first story. For NS motions, the reduction is significantly larger at the east side of the building than at the west side and center, both in the first story (75% as compared to 44% at the west side and 0% at the center) and above (63% as compared to 47% at the west side and 43% at the center), which is consistent with the spatial distribution of the observed damage (Fig. 6). One discrepancy between the observed damage and the reduction of stiffness estimated form travel times is that the former indicates no major cracks in the upper part along the west side and center of the building, while the latter suggests significant reduction of stiffness (47% and 43%). This discrepancy is likely due to damage in the upper part that was not easily visible and hence was not recorded.

Next, we examine the reduction of floor stiffness vs. time. Fig. 14 shows the floor stiffness, as a fraction of the initial stiffness, for EW motions (top) and NS motions (bottom). The curves represent linear interpolation between the representative interval values, assigned to the central time of the window. We note here that the interval values are weighted averages of the instantaneous values within the time window. Hence, damage that occurred near the end of the second time window would not contribute much to the weighed average for that window, but would reflect on the interval value for the third time window. In view of this fact, the changes in stiffness in Fig. 14 suggest that, most of the reduction of stiffness in the EW direction started to occur, or occurred relatively early within the time window. The same is true for the reduction of stiffness in the NS direction everywhere in the upper part of the building, while in the first story, at both ends of the building, the NS stiffness changed significantly near the end of the second time window, especially at the east end. This is consistent with the timing of the collapse of the first story columns in row F, which occurred at the very end of the second time interval (at about 11.2 s [8]), and affected mostly the 1st floor NS stiffness at the east side of the building. The first story NS stiffness did not change at the center of the building.

The two horizontal lines in Fig. 14 correspond to values obtained by Kojić et al. [9] for two models using the readily available structural analysis software at that time—ETABS, which was linear. Due to this limitation of the software, they analyzed the three-dimensional (3D) nonlinear response of the building using equivalent linear elastic models. They accounted for the effects of the flexibility of the soil and the soil–structure interaction, by adding a fictitious story beneath ground level. Their Model II_A considered the full stiffness of all structural members, i.e. the initial state of the building, while their model II_B considered reduced stiffness, to account for the effects of nonlinear structural response and damage. In particular, they reduced the moments of inertia of some columns at the ground level, but did not change their axial stiffness, and did not change the stiffness of the structural elements above the 2nd floor. The reduction of the moments of inertia was 70% for the columns along lines A, B, E, and F (see Fig. 4, top), and 20% for those along lines C and D. Further, they introduced hinge supports for columns E1, E4 and for all columns on the line F, at ground level. The resulting frequencies of vibration for Model II_A were 0.91 Hz for EW motions, and 1.64 Hz for NS motions, and for Model II_B they were 0.80 Hz for EW motions and 1.61 Hz for NS motions, all shown, by horizontal lines in Fig. 15. The reductions of stiffness in the first story columns by 20% or 70% are also indicated in Fig. 14 by wide horizontal lines. The qualitative agreement of the characteristics of the ETABS model chosen by Kojić et al. [9] with the results of the present study is excellent.

3.5. Fundamental fixed-base frequency estimates from wave travel times

The changes in travel times from one time window to another can be cast into changes in the interference conditions, which relate to the fundamental *fixed-base* period of vibration of a shear beam, T_1, and the corresponding frequency $f_1 = 1/T_1$. Assuming a 1D model and deformation in shear only, the height of the building above ground level is 1/4 of the wavelength, which gives

$$T_1 = 4\tau_{\text{tot}}, \tag{6}$$

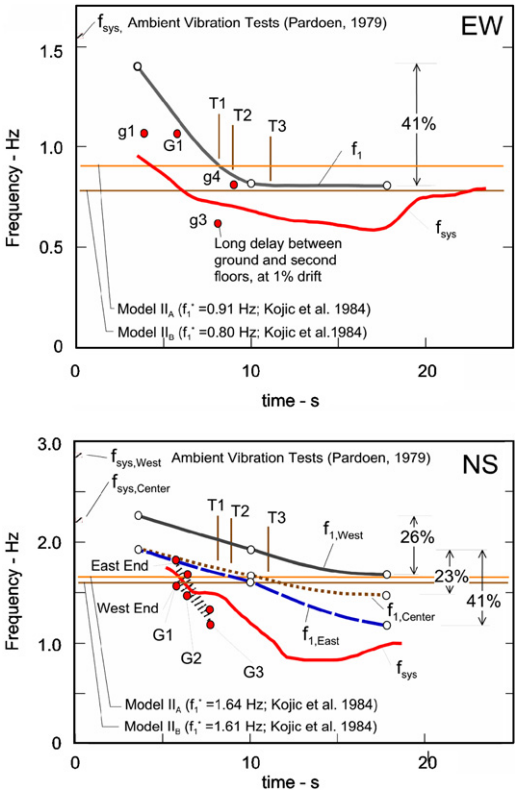

Fig. 15. Frequency of vibration for EW (top) and NS (bottom) motions: comparison of results from different studies.

where τ_{tot} is the time it takes for the input impulse to traverse the height of the building. Also, as $\tau_{\text{tot}} = \sum_i \tau_i$, $T_1 = \sum_i (4\tau_i)$, and $f_1 = 1/\sum_i (4\tau_i)$. We note here that, because of the assumption that the motion of the building consists of *vertically* propagating waves, due to *shear* deformation only, the estimated values of f_1 from travel times are lower bounds.

We computed T_1 and f_1 from travel times using Eq. (6) for EW motions, for which a 1D wave propagation model appears to be appropriate. We also computed T_1 and f_1 from the NS motions travel times for the west side, center and the east side of the building. The NS response was clearly two dimensional (2D) and asymmetric. Hence, most meaningful of these frequencies is f_1 for the center of the building, as the closest one to the fundamental fixed-base frequency for NS translation, while we use the other two values, for the sides of the building merely as measures of the stiffness of the building at both sides. The values for τ_{tot}, T_1, and f_1 are summarized in Table 5 for the three time windows. For the second and third time windows, the percentage change in frequency and in rigidity of a corresponding 1D equivalent uniform shear beam are also given.

It can be seen that the overall EW stiffness of the structure was reduced by 65%. The overall NS stiffness was reduced by 46% at the west side of the building, by 41% at the center, and by 65% at the east side. The largest decrease at the east side of the building, as suggested by the analysis of travel times, is consistent with the observed damage. The initial values of f_1 and the implied changes in the overall stiffness are shown also in the sketches in Figs. 12 and 13.

Fig. 15 shows graphically the changes of f_1 with time for EW (top) and NS (bottom) motions, and compares f_1 from travel times with other estimates of f_1 and of the soil–structure system frequency, f_{sys}. The open circles show f_1 from travel times at the center of the corresponding time interval, and the line connecting the circles represents interpolated values. The other estimates include: (1) the system frequencies, f_{sys}, measured from ambient vibration tests conducted before the Imperial Valley earthquake [24],

Table 5
Equivalent shear wave velocities of a uniform shear beam, v_{eq}, and fundamental fixed-base frequencies of vibration, f_1, for the three time windows, estimated from mean wave travel times τ_{tot} over the building height ($f_1 = 1/(4\tau_{\text{tot}})$), for EW motions, and for NS motions recorded at the West end, center, and East end of the building. The percentage changes in f_1 and the equivalent rigidity are also shown

Motion	Side	$t<7$ s			$7<t<13$ s					$t>13$ s				
		(1a)	(1b)	(1c)	(2a)	(2b)	(2c)	(2d)	(2e)	(3a)	(3b)	(3c)	(3d)	(3e)
		τ_{tot} (s)	v_{eq} (m/s)	f_1 (Hz)	τ_{tot} (s)	v_{eq} (m/s)	f_1 (Hz)	$\Delta f_1/f_{\text{ref}}$ (%)	$\Delta\mu/\mu_{\text{ref}}$ (%)	τ_{tot} (s)	v_{eq} (m/s)	f_1 (Hz)	$\Delta f_1/f_{\text{ref}}$ (%)	$\Delta\mu/\mu_{\text{ref}}$ (%)
EW	Center	0.18	142	1.39	0.31	82	0.81	−42	−66	0.305	84	0.82	−41	−65
NS	West	0.11	232	2.27	0.13	196	1.92	−15	−28	0.15	170	1.67	−26	−46
	Center	0.13	196	1.92	0.15	170	1.67	−13	−24	0.17	150	1.47	−23	−41
	East	0.13	196	1.92	0.16	159	1.61	−16	−30	0.22	116	1.14	−41	−65

(2) "instantaneous" system frequency f_{sys} estimated from the recorded response to the 1979 Imperial Valley earthquake using Gabor transform [7], (3) "first mode" frequencies of the soil–structure system f_1^* estimated from two equivalent linear ETABS models, II_A and II_B, (shown by horizontal lines [9]), and (4) "instantaneous" fixed-base frequency f_1 estimated from travel times of high frequency pulses using decomposition of the response to the Imperial Valley earthquake in a wavelet basis (shown by solid dots [8]). The vertical lines, T1, T2, and T3, show the times when major damage occurred, as estimated from the analysis of novelties in the recorded response to the Imperial Valley earthquake [8].

The system frequencies, f_{sys}, measured by ambient vibration tests [24] are shown along the left edge of the plots (by a short hatched line). These values are 1.54 Hz for EW motions, 2.24 Hz for NS motions at the center of the building, and 2.81 Hz for NS motions at the west side, which was interpreted as the first torsional frequency. It is noted here that the ambient vibration measurements [24] were made without using a reference site. Consequently, the measured structural frequencies may not be accurate due to influence from the site frequencies.

We first examine the consistency of the different estimates of frequency for EW motions. It can be seen from Fig. 15 (top) that the interpolated interval estimates of f_1 during the earthquake are always higher than the moving window estimates of f_{sys} during the earthquake. This is as would be expected, in view of the fact that the two frequencies are related by

$$f_{sys}^{-2} = f_1^{-2} + f_H^{-2} + f_R^{-2}, \tag{7}$$

where f_H and f_R represent the horizontal and rocking frequencies of a rigid building on flexible soil, which implies that f_{sys} is smaller than the smallest of f_1, f_H or f_R. The value of f_{sys} during the ambient vibration tests is higher not only than f_{sys} during the earthquake shaking, but also higher than f_1 during the earthquake shaking, which can be explained by the very small amplitudes of the response, excited by cultural noise and wind.

Next we examine the relationship between the interpolated *interval* estimates of f_1 from impulse responses travel times and the *instantaneous* estimates of f_1 from travel times of high frequency pulses identified in the analysis of novelties [8]. It can be seen that for all of the identified pulses, the *instantaneous* estimates of f_1 are lower than the *interval* estimates of f_1, but are still higher than the moving window estimates of f_1, except for pulse g3. The lower *instantaneous* f_1 from novelties could be explained by the fact that (a) these values are representative of very short time intervals, and hence exhibit larger fluctuations than the smoother *interval* values, which are averages over much longer time windows, and (b) they were typically measured during extreme drift amplitudes (e.g., pulse g3 occurred at a time of about 1% first story drift). Events T1, T2, and T3 were associated with the times of major damage [9]. The time of the significant fall in the values of f_1 are consistent with the times of T1, T2, and T3.

Similar observations can be made for the different estimates of the frequencies for NS motions, shown in Fig. 15 (bottom). Due to the larger stiffness at the west side of the building, relative to the center (additional shear wall between the 2nd floor and roof), the corresponding initial value of f_1 is larger than that for the center. The initial value of f_1 for the east side is also smaller than for the west side, due to the absence of a shear wall on line F at the ground floor (Fig. 3, top). The NS system frequency, which was estimated from the recorded earthquake response at the center, and is hence denoted by $f_{\text{sys, Center}}$ is always smaller than $f_{\text{1, Center}}$. It can also be seen that the system frequencies from ambient vibration tests measured from the response at the west side and at the center are higher than the corresponding initial values of f_1 during the earthquake shaking, which can be explained by the very small amplitudes of response to ambient noise.

4. Summary and conclusions

This paper explored a structural health monitoring method, based on detecting changes in stiffness of the structural members by measuring changes in wave travel times of seismic waves propagating through these members. The wave travel times were measured from impulse response functions computed from the recorded horizontal response during the earthquake in three time windows—before, during, and after the occurrence of the major damage, using the first time window as reference. Hence this method does not rely on baseline data measured before the earthquake, or model based predictions of the response for different damage scenarios. A further and major advantage of this method is that *it is local*, as opposed to the modal methods, which are global, and hence can point out to the location of the damage with data from fewer sensors than the methods that detect changes in mode shapes. This method is examined using earthquake response data recorded in a full-scale building damaged by the earthquake.

The method is presented and applied in its most rudimentary form, based on several assumptions. One assumption is that one-dimensional wave propagation up and down the structure can capture the principal features of the response, and that side reflections of the non-vertically propagating waves [20–22] can be neglected. Another assumption is that it is sufficient to work only with the recorded horizontal translations. Further assumptions are that one can neglect: the wave propagation effects associated with the seismic waves incident horizontally through the foundation [25,26], the structural response resulting from warping and deformation of the foundation [27], and the rotational waves in the building caused by soil–structure interaction. Also, the detailed nature of the

contributions of torsion and of rocking to the recorded transverse (NS) translations was not explicitly considered.

The results show that, despite the simplifying assumptions, for this building, even for time windows as short as 5 s, the method yields meaningful impulse responses and wave travel times between sensors. The inferred spatial distribution of the initial shear wave velocities throughout the building is consistent with the actual distribution of stiffness, and the spatial distribution of the *changes* in stiffness is generally consistent with the observed damage. Further, the fundamental fixed-base frequencies, f_1, and their changes, estimated from the measured travel times, are consistent with other estimates of frequency, such as the ''instantaneous'' soil–structure system frequency, f_1, during the earthquake measured from time–frequency distributions of the energy of the recorded response, estimated from simulations of the seismic response using ETABS equivalent linear models, and measured from ambient vibration tests data. Comparison of f_1 and f_{sys} during the earthquake shows that $f_1 > f_{sys}$, during the entire shaking, as it should be due to the soil–structure interaction, which affects f_{sys} but not f_1.

It is concluded that the analysis of wave travel times in a building undergoing damaging response, measured from impulse response functions computed from recorded seismic response in different time windows during the earthquake, can provide useful information about the degree and spatial distribution of the changes in the component stiffness. The spatial resolution of the method would depend on the number and the separation distance of the sensors, and its temporal resolution—on the length of the time windows. This method can be a useful tool for structural health monitoring, and therefore should be further improved and refined. This method can also be used to estimate the attenuation of seismic waves propagating through the structure and the structural damping [6,17,18], which is left for future work.

Acknowledgements

The seismic monitoring array in the ICS building was operated by California Geological Survey (formerly California Division of Mines and Geology).

References

[1] Chang PC, Flatau A, Liu SC. Review paper: health monitoring of civil infrastructure. Struct Health Monitoring 2003;2(3):257–67.

[2] Doebling SW, Farrar CR, Prime MB, Shevitz DW. Damage identification and health monitoring of structural and mechanical systems from changes in their vibration characteristics: a literature review. Report LA-13070-MS, Los Alamos National Laboratory, Los Alamos, NM, 1996.

[3] Kanai K. Some new problems of seismic vibrations of a structure. In: Proceedings of Third World Conference Earthquake Engineering, Auckland and Wellington, New Zealand, January 22–February 1, 1965. p. II-260–75.

[4] Todorovska MI, Trifunac MD, Ivanović SS. Wave propagation in a seven-story reinforced concrete building, Part I: theoretical models. Soil Dyn Earthquake Eng 2001;21(3):211–23.

[5] Todorovska MI, Trifunac MD, Ivanović SS. Wave propagation in a seven-story reinforced concrete building, Part II: observed wavenumbers. Soil Dyn Earthquake Eng 2001;21(3): 225–36.

[6] Snieder R, Şafak E. Extracting the building response using interferometry: theory and applications to the Millikan Library in Pasadena, California. Bull Seism Soc Am 2006;96(2): 586–98.

[7] Todorovska MI, Trifunac MD. Damage detection in the Imperial County Services Building I: the data and time–frequency analysis. Soil Dyn Earthquake Eng 2007;27(6):564–76.

[8] Todorovska MI, Trifunac MD. Damage detection in the Imperial County Services Building II: analysis of novelties via wavelets. Soil Dyn Earthquake Eng 2007, submitted for publication.

[9] Kojić S, Trifunac MD, Anderson JC. A post earthquake response analysis of the Imperial County Services building in El Centro. Report CE 84-02. University of Southern California, Department of Civil Engineering, Los Angeles, CA, 1984.

[10] Şafak E. Detection of seismic damage in multi-story buildings by using wave propagation analysis. In: Proceedings of sixth US National Conference on Earthquake Engineering, EERI, Oakland, CA, Paper No. 171, 1998. p. 12.

[11] Ivanović SS, Trifunac MD, Todorovska MI. On identification of damage in structures via wave travel times. In: Erdik M, Celebi M, Mihailov V, Apaydin N, editors. In: Proceedings of NATO advanced research workshop on Strong-Motion Instrumentation for Civil Engineering Structures, June 2–5, 1999. Istanbul, Turkey: Kluwer Academic Publishers; 2001. p. 447–68.

[12] Trifunac MD, Ivanović SS, Todorovska MI. Wave propagation in a seven-story reinforced concrete building, Part III: damage detection via changes in wavenumbers. Soil Dyn Earthquake Eng 2003; 23(1):65–75.

[13] Ma J, Pines DJ. Damage detection in a building structure model under seismic excitation using dereverberated wave machines. Eng Struct 2003;25:385–96.

[14] Oyunchimeg M, Kawakami H. A new method for propagation analysis of earthquake waves in damaged buildings: evolutionary Normalized Input–Output Minimization (NIOM). J Asian Architecture Build Eng 2003;2(1):9–16.

[15] Todorovska MI, Trifunac MD. Impulse response analysis of the Van Nuys 7-storey hotel during 11 earthquakes and earthquake damage detection. Struct Control Health Monit 2007, in press; doi:10.1002/stc.208.

[16] Kawakami H, Haddadi HR. Modeling wave propagation by using normalized input–output minimization (NIOM). Soil Dyn Earthquake Eng 1998;17(2):117–26.

[17] Kawakami H, Oyunchimeg M. Normalized input–output minimization analysis of wave propagation in buildings. Eng Struct 2003;25(11):1429–42.

[18] Kawakami H, Oyunchimeg M. Wave propagation modeling analysis of earthquake records for buildings. J Asian Architecture Build Eng 2004;3(1):33–40.

[19] Kohler MD, Heaton T, Bradford SC. Wave propagation in buildings. Bull Seism Soc Am 2007;97(4):1334–45.

[20] Todorovska MI, Trifunac MD. Antiplane earthquake waves in long structures. J Eng Mech ASCE 1989;115(12):2687–708.

[21] Todorovska MI, Trifunac MD. A note on the propagation of earthquake waves in buildings with soft first floor. J Eng Mech ASCE 1990;116(4):892–900.

[22] Todorovska MI, Lee VW. Seismic waves in buildings with shear walls or central core. J Eng Mech ASCE 1989;115(12):2669–86.

[23] Şafak E. Wave propagation formulation of seismic response of multi-story buildings. J Struct Eng ASCE 1999;125(4):426–37.

[24] Pardoen GC. Imperial County Services Building: ambient vibration test results. Report No. 79-14, University of Canterbury, Department of Civil Engineering, New Zealand, 1979.

[25] Trifunac MD, Ivanović SS, Todorovska MI, Novikova EI, Gladkov AA. Experimental evidence for flexibility of a building foundation supported by concrete friction piles. Soil Dyn Earthquake Eng 1999;18(3):169–87.

[26] Trifunac MD, Gičev V. Response spectra for differential motion of columns, paper II: out-of-plane response. Soil Dyn Earthquake Eng 2006;26(12):1149–60.

[27] Gičev V. Investigation of soil-flexible foundation–structure interaction for incident plane SH waves. PhD Dissertation, Department of Civil Engineering, University Southern California, Los Angeles, CA, 2005.